

3D Patient Specific Models of the Circle of Willis

Moore, S.M.¹, David, T.¹ and Fink, J.²

¹ Centre for Bioengineering, University of Canterbury, Christchurch

² Otago School of Medicine and Health Sciences, University of Otago, Christchurch

Email: steve.moore@canterbury.ac.nz

Keywords: computational biofluid mechanics, circle of Willis, autoregulation, cerebral flow

EXTENDED ABSTRACT

The Circle of Willis (*CoW*) (Figure 1) is a ring-like arterial structure located at the base of the brain. It is the major arterial anastomoses in the brain and is responsible for the distribution of oxygenated blood throughout the cerebral mass. The Internal Carotid (*ICA*) and Basilar (*BA*) arteries bring blood into the *CoW* and are termed *afferent* arteries. The Anterior (*ACA*), Middle (*MCA*), and Posterior (*PCA*) cerebral arteries transport blood away from the *CoW* and are termed *efferent* arteries. The circle is completed by one anterior (*ACoA*) and two posterior (*PCoA*) *communicating* arteries which allow for blood to be rerouted in order to maintain oxygen supply to the cerebral tissue in the event that blood supply through any of the *afferent* arteries be reduced.

Among the general population, only approximately 50% have a complete *CoW* (Hartkamp et al. (1998), Alpers et al. (1959)), where absent or hypoplastic vessels are common, among a multitude of possible anatomical variations, reducing the degree to which blood may be rerouted. While an individual with one of these variations may under normal circumstances suffer no ill effects, there are certain pathological conditions which can present a risk to the person's health and increase the possibility of suffering an ischaemic stroke when compounded with the effects of an anatomical variation. Clinical scenarios which may benefit from mathematical modelling of flow patterns throughout the *CoW* include the prediction of how far a hypertensive patient's blood pressure could safely be reduced before lowering cerebral perfusion to a potentially dangerous level. This is a common clinical question and current theory on the treatment for hypertension is to be quite aggressive in the reduction in blood pressure, but not being able to predict the effects on cerebral perfusion limits the ability of the clinician to use an aggressive treatment of anti-hypertensive drugs. Since hypertension and atherosclerosis are linked, it would be a common finding for a hypertensive patient to have some degree of stenosis in one or more of their *afferent* arteries, in which case

lowering the overall systemic blood pressure could

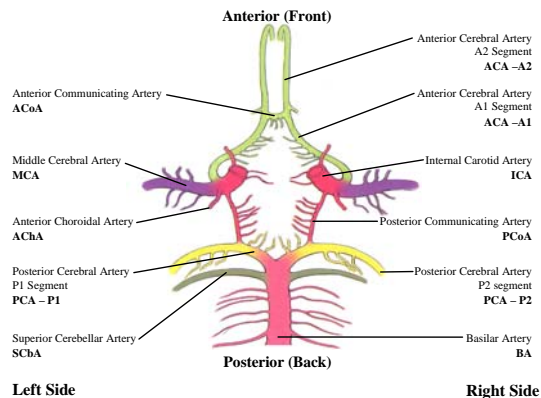


Figure 1. Schematic of the circle of Willis.

have a more significant effect on flow patterns throughout region of the circle of Willis perfused by the stenosed artery. Other important clinical scenarios which would benefit from mathematical modelling include surgical procedures where an *afferent* artery is occluded, either temporarily or permanently, in which case the maintenance of oxygen delivery to the cerebral mass is completely reliant on the *CoW* to provide collateral flow.

Using in-house interactive software, incorporating a variation of a standard marching cube algorithm, 3D patient specific models of the circle of Willis may be rapidly segmented from the MRI Time of Flight data, into which the equations governing fluid flow can be solved. The results of the numerical fluid simulations can provide detailed information regarding the haemodynamic response of an individual to certain pathological conditions, such as the build up of atherosclerotic plaque on the walls of the *afferent* arteries or even complete occlusion of an artery and predict whether ischaemia is likely to occur. The computer model implements an advanced cerebral autoregulation mechanism that mimics the ability of the arterioles in the brain to vasodilate or constrict in response to an alteration in cerebral perfusion pressure via the alterations in oxygen and carbon dioxide in the cerebral tissue, such that a constant cerebral blood flow can be maintained.

1. INTRODUCTION

Previous work available in the literature has focused on modeling the flow patterns in the CoW in 1D (Hillen et al. (1986), Charbel et al. (2004)), 2D (David et al. (2003)), and in 3D (Cebral et al. (2003)). Furthermore, there has been a significant body of research focused on creating mathematical models of the physiological control system regulating cerebral perfusion, known as cerebral autoregulation (Thoman et al. (1998), Ursino et al. (1991), Banaji et al. (2005)). To date however, there has been little effort focused on the integration of models of the circle of Willis geometry with a cerebral autoregulation model, and furthermore, tailoring the modeling technique to simulate the aforementioned clinical scenarios. The work presented here outlines a method whereby 3D models of the circle of Willis may be directly segmented from Time of Flight (*TOF*) MRI data and combined with Phase Contrast (*PC*) MRI measurements of blood flow through the efferent arteries to generate patient specific simulations of the response to occlusions of the afferent arteries. The model uses the novel approach of porous blocks to represent the effects of the arteriole and capillary beds (David et al. (2003)), and the major efferent arteries have therefore been terminated a short distance downstream of the circle with a porous block at each efferent artery's termination. This block represents a resistance to the flow with the same attributes as the capillary bed such that realistic representations of the flow can be achieved. A sample case of a normal complete CoW is considered examining stenosis in combination with occlusion in the ICAs.

2. METHODS

2.1. Geometry Generation

The geometry generation was accomplished with the creation of in-house, interactive software for generating patient specific models of the circle of Willis. The software includes the ability to specify arbitrarily shaped regions of interest and either remove noise, enhance the voxel intensity, apply Gaussian smoothing, within these regions, acting on either the entire dataset, or slice by slice. Following the enhancement of the MRI dataset a variation of a standard marching cube algorithm (Lorensen et al. (1987)) is implemented, allowing the 3D geometries to be directly segmented from the 3D MRA dataset (Figure 2).

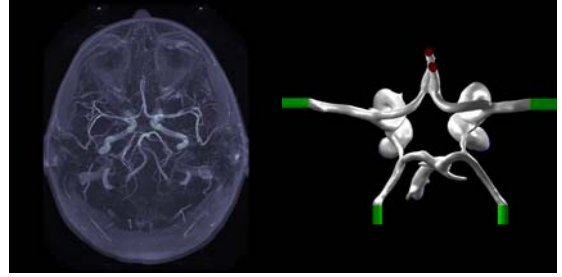


Figure 2. A TOF MRI scan and the resulting segmented model. Note: the porous blocks are illustrated in green.

In order to simulate stenoses, the afferent arteries have been extruded from their truncation in a similar manner to the porous blocks extruded at the ends of the efferent arteries. Using the in-house software, the extruded arteries can be individually selected and reshaped (Figure 3) to simulate the effects of a stenosis, using the relation:

$$\mathbf{R}_{\text{sten}} = \mathbf{R}_{\text{orig}} + \text{DoS} (\mathbf{R}_{\text{cent}} - \mathbf{R}_{\text{orig}}) e^{-\alpha(z - z_{0.5})} \quad (1)$$

where z represents the axial coordinate of a vertex comprising the surface triangulation along the extrude and $z_{0.5}$ the coordinate midway along the extrude, \mathbf{R}_{orig} is the original vector in the xy plane between the centreline of the extrude and a given vertex and \mathbf{R}_{cent} is the coordinate of the centreline, \mathbf{R}_{sten} is the new value for the stenosed vessel, α is a scaling parameter controlling the profile of the stenosis, and DoS is the user specified degree of stenosis. This approach has the useful feature of applying to arterial cross sections which are not perfectly circular, as is found with models based on medical imaging data.

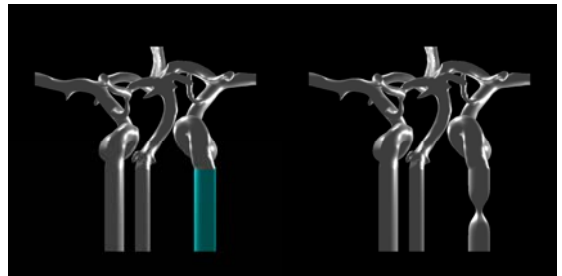


Figure 3. An example afferent artery extrude and the resulting stenosis imposed on the geometry.

Although physically, carotid stenosis more commonly occurs farther upstream at the level of the carotid bifurcation where the ICA originates, the assumption is made for the present study that the dominant effect of the stenosis is its reduction

in cross-sectional area, rather than its placement along the ICA.

2.2. Cerebral Autoregulation Model

The two main features of the brains' cerebral autoregulation mechanism which need to be captured mathematically in order to physiologically simulate changes in cerebral blood flow (*CBF*), are the transient response (Figure 4a) and the limits of mean arterial blood pressure (*MABP*) within which the mechanism is effective (Figure 4b). The nature of the dynamics comes from a study performed by Newell et al. (1994) where a step reduction in MABP was induced in a number of volunteers with a thigh-cuff-test maneuver and CBF was monitored using Transcranial Doppler Ultrasonography (*TCD*).

As is illustrated in Figure 4a the CBF exhibits first order dynamics, gradually returning to its set point over a period of approximately 20 seconds as the cerebrovascular resistance (*CVR*) adjusts. The limits of autoregulation come from a study performed by Strandgaard et al. (1976) where MABP was reduced in a number of volunteers in a series of steps, by infusion of trimethaphan camsylate in combination with a head-up-tilt maneuver, while CBF was monitored. The results showed that despite the variations in an individuals actual MABP, their lower limit of autoregulation would be reached when MABP was reduced by approximately the same proportion. For the normotensive subgroup examined in the study, the lower limit was achieved following a 74% reduction in MABP.

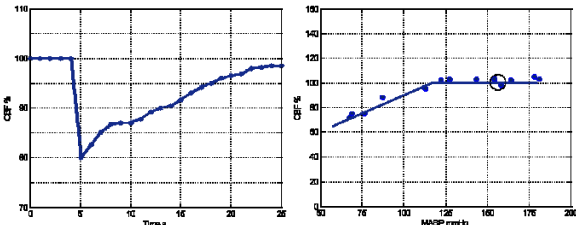


Figure 4. Example data illustrating autoregulation dynamics and an autoregulation lower limit.

The autoregulation model assumes CVR to be a function of the CO₂ levels in the brain tissue, where the dynamics are modelled as:

$$\frac{dC_tCO_2}{dt} = CMRO_2 + CBF(C_aCO_2 - C_tCO_2) \quad (2)$$

where C_tCO_2 is the tissue concentration of carbon dioxide, C_aCO_2 is the arterial concentration of carbon dioxide (assumed to be 0.49mL/mL) and

$CMRO_2$ is the metabolic rate of oxygen consumption (assumed to be 0.035mL/g/min for all parts of the brain), which due to the stoichiometry of the aerobic metabolism in the brain tissue, is equal to the cerebral metabolic rate of carbon dioxide production. The driving cause for CVR to alter is subsequently given by an autoregulation activation, Aut_{CVR} which is a function of the difference in tissue CO₂ levels:

$$\frac{dAut_{CVR}}{dt} = G_{CVR}(C_tCO_{2sp} - C_tCO_2) \quad (3)$$

where G_{CVR} is the proportional gain (taken as 7 in order to reproduce the time scales illustrated in Figure 3a) and the set point sp for CO₂ in the tissue is given by the steady state solution of (2) as:

$$C_tCO_{2sp} = C_aCO_2 + \frac{CMRO_2}{CBF_{av}} \quad (4)$$

By definition, the set points for tissue CO₂ occur when CBF is also at its set point. The reason for separating out the actual resistance from its driving force (tissue CO₂) is to allow for a more elegant approach to incorporating the limits of autoregulation, given as:

$$CVR = \frac{CVR_{ll} + CVR_{ul}e^{(Aut_{CVR}-C)}}{1 + e^{(Aut_{CVR}-C)}} \quad (5)$$

so that CVR becomes a sigmoidal function of Aut_{CVR} with upper and lower limits CVR_{ll} and CVR_{ul} . The constant C is defined as:

$$C = -\log\left(\frac{CVR_{sp} - CVR_{ll}}{CVR_{ul} - CVR_{sp}}\right) \quad (6)$$

such that with zero autoregulation activation, CVR is at its set point. Also included in the model is a dynamic for the clinical variable known as oxygen extraction fraction (*OEF*). While not strictly a part of cerebral autoregulation, it is closely associated with it, and is vitally important if oxygen delivery to the brain tissue is the primary feature under investigation. OEF is the amount of oxygen available in the arterial blood, which is actually consumed by the brain tissue and under normal circumstances, is of the order of 30 – 40%. It therefore provides another backup mechanism for preventing ischemic conditions by allowing more oxygen to be extracted from the arterial blood, if CBF cannot be restored to its set point. Using a similar approach to the CVR model, the OEF activation is modelled using an activation Aut_{OEF} as which is a function of the difference in oxygen delivery to the brain tissue, from the brains CMRO₂:

$$\frac{dAut_{OEF}}{dt} = G_{OEF}(CMRO_2 - CBF \cdot C_aO_2 \cdot OEF) \quad (7)$$

(7)

where G_{OEF} is a proportional gain (taken as 100) and C_aO_2 is the oxygen concentration in arterial blood (assumed to be 0.21mL/mL). The limits of OEF are modelled using a similar sigmoidal function as for CVR:

$$OEF = \frac{OEF_{ll} + OEF_{ul}e^{(Aut_{OEF}-O)}}{1 + e^{(Aut_{OEF}-O)}} \quad (8)$$

where intuitively the lower limit of oxygen extraction is zero and the upper limit is taken as 77%. The constant O has the same effect as C in (6), and is evaluated in the same manner as (6) with OEF replacing CVR.

2.3. Governing Equations

In order to model the blood flow throughout a circle of Willis, the governing equations are the conservation of mass:

$$\int_{CS} \rho \mathbf{u} \cdot d\mathbf{A} = 0 \quad (9)$$

And the conservation of momentum:

$$\begin{aligned} \frac{\partial}{\partial t} \int_{CV} \rho \mathbf{u} dV + \int_{CS} \rho \mathbf{u} \mathbf{u} \cdot d\mathbf{A} = \\ - \int_{CV} \nabla p dV + \int_{CS} \eta \nabla \mathbf{u} \cdot d\mathbf{A} - \int_{CV} \eta \mathbf{u} CV R dV \end{aligned} \quad (10)$$

As these two equations are commonplace in any fluid dynamics modelling, it is assumed that their meaning is understood and the only two terms worthy of elaboration are the first and last terms on the right hand side of (10). The non-Newtonian blood viscosity η is modelled using the Carreau-Yasuda model:

$$\frac{\eta(\dot{\gamma}) - \eta_\infty}{\eta_0 - \eta_\infty} = \left(1 + (\lambda \dot{\gamma})^a\right)^{\frac{n-1}{a}} \quad (11)$$

where η_0 is the zero-shear viscosity and η_∞ the infinite shear viscosity, taken as 0.1518 Pa.s and 0.00348 Pa.s respectively and $\dot{\gamma}$ is the strain rate magnitude. The remaining constitutive parameters λ , a , and n are taken as 40.0s, 2.0 and 0.356 respectively (Kim et al. (2006)). The last term on the right hand side of (10) is an extra body force term which is applied only in the fluid domain occupied by the porous blocks and is essentially Darcy's law for porous media. The CVR determined by the cerebral autoregulation model is input into the body force term at every timestep during the simulation in order to regulate CBF. It is important to note that the six CVR values applied in momentum equation within the porous

blocks of the six efferent arteries bear no resemblance to a Poiseuille type resistance that could be simply related to pressure difference and flowrate, rather, they are best thought of as the reciprocal of the permeability term in Darcy's law.

In performing the simulations the patient specific CVR values required to achieve the normal CBF values are not generally known in advance and have to be determined during the simulation. An initial guess of 1000 mm⁻² would hence be specified at the start of the simulation, and the autoregulation mechanism allowed a period of time to alter the CVR values until the normal CBF levels are achieved. At this point the current CVR in each porous block could be set as CVR_{sp} . The lower limit of autoregulation can be found using a similar approach, but with the afferent pressure reduced to 74% of its normal level.

2.4. Boundary Conditions

Given the assumptions for C_aCO_2 and $CMRO_2$ the set points for the C_tCO_2 in each efferent artery require a measurement of CBF under normal conditions. In this case *CINE* phase contrast magnetic resonance imaging (*PC MRI*) measurements are utilized in order to measure CBF in each efferent artery.

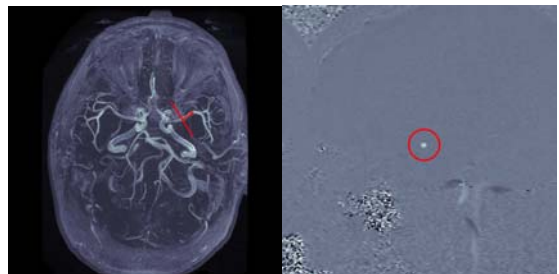


Figure 5. A TOF MRI dataset illustrating the positioning of an imaging plane normal to the RMCA, and the corresponding image from a PC scan illustrating the velocity data.

Following the patients' TOF scan, the MR image of the cerebral vasculature can be used as a reference for positioning the imaging plane normal to an efferent artery (Figure 5a). With the development of in-house interactive software, a region of interest (*ROI*) can be drawn around the artery of interest (Figure 5b) and the CBF computed at each point in the cardiac cycle as:

$$CBF(t) = \int_{ROI} \mathbf{u}(t) \cdot d\mathbf{A} \approx \sum_{ROI} u_{pix}^t A_{pix}^t \quad (12)$$

(where pix indicates a pixel velocity or area), from which the average value CBF_{av} , to be used in the calculation of C_iCO_{2sp} in (4) can be calculated as:

$$CBF_{av} = \frac{1}{T_{cyc}} \sum_{t=1}^{N_{cyc}} \frac{CBF^t - CBF^{t-1}}{2} \Delta t \quad (13)$$

Where T_{cyc} and N_{cyc} represent the time period of the cardiac cycle and the number of points measured within the cardiac cycle. The encoding velocities chosen (V_{enc}) were 70cm/s for the ACAs and PCAs and 80cm/s for the MCAs with 30 points throughout the cardiac cycle specified.

Inlet pressure waveforms of 120 over 80mmHg are imposed on the afferent artery inlets and a capillary bed pressure of 30mmHg is imposed on the efferent outlets (the downstream face of the porous blocks). The inlet pressure waveforms were generated by taking the afferent CBF waveforms and mapping the peak systolic and diastolic flowrates to a pressure of 120 over 80mmHg and linearly interpolating all points in between.

The simulations were performed with the finite volume solver Fluent™ version 6.2.16 using the segregated-implicit solver, first order upwinding, node-based gradient reconstruction, SIMPLE pressure-velocity coupling and second order implicit time integration schemes with a timestep size of 0.04s. The cerebral autoregulation model was discretized with a Runge-Kutta 4th order scheme.

3. RESULTS

The results presented here are a sample case for a normal complete CoW, subjected to unilateral stenoses in the ICA's in combination with varying degrees of stenosis in the remaining two afferent arteries. The results are presented by means of radial plots, displaying clinical variables for the cerebral territories supplied by the six efferent arteries at the end of each simulation. The blue dashed hexagons in the CVR and OEF radial plots indicate the lower limit of autoregulation and upper limits of oxygen extraction respectively.

3.1. LICA Occlusion

The results for the autoregulatory response to the LICA occlusion in combination with a unilateral stenosis are presented in Figure 6. It can be observed that the effects of the LICA occlusion and the other stenoses result in efferent CBF not being completely restored in the LACA and LMCA ipsilateral to the occlusion as CVR in these arteries approaches the lower limit of

autoregulation (Figure 5b). As a result, $CtCO_2$ for these two arteries remains elevated following the simulations. An important point to note is that CVR did not in fact reach the lower limit because

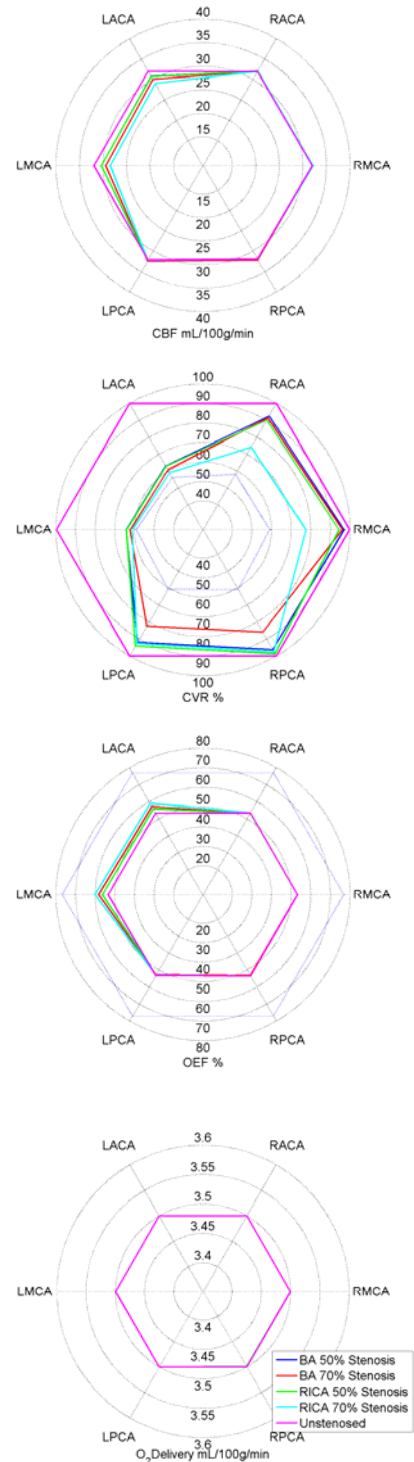


Figure 6. The end response to an occlusion of the LICA in combination with other unilateral stenoses for the complete CoW displaying efferent CBF, CVR, OEF, and O_2 delivery.

the 20s allowed for the simulation was not enough time for CVR to reduce to the lower limit. This result was found in a number of simulations and proportional controller and as the CBF returns to its normal level, then so diminishes the drive for a

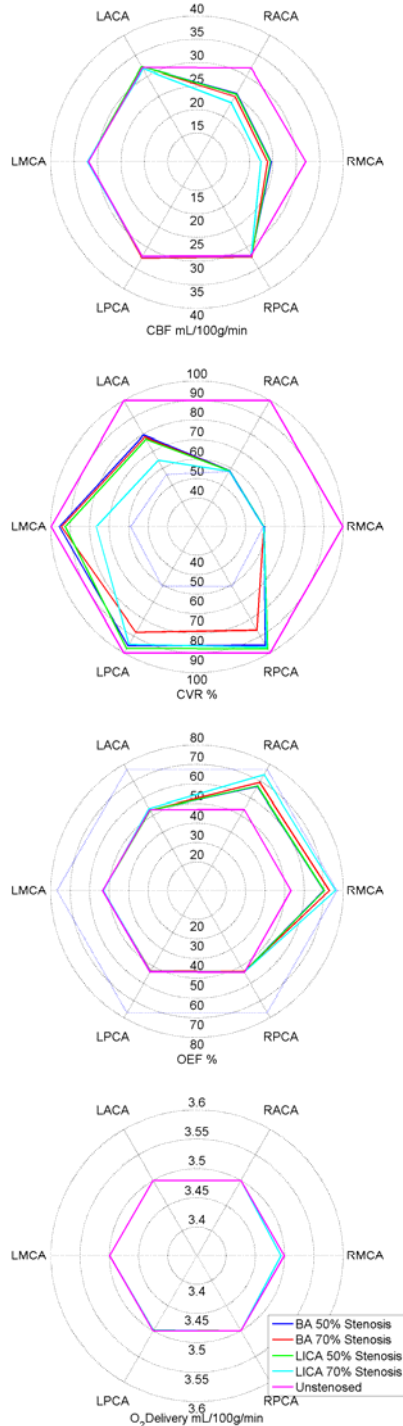


Figure 7. The end response to an occlusion of the RICA in combination with other unilateral stenoses for the complete CoW displaying efferent CBF, CVR, OEF, and O₂ delivery.

further reduction in CVR. Given more simulation time, these two efferent flowrates may in fact return to their normal value, but the important result is that as can be observed in Figure 5d, there is only a small increase in OEF required to maintain O₂ delivery to these arteries, which is the major result of the simulation. In cases where the occlusion and stenosis result in a very dramatic reduction in CBF, the lower limit of autoregulation will actually be reached and this will occur very quickly. It can also be observed that the 70% RICA stenosis has a much greater effect on the efferent flood flow through the contralateral RACA and RMCA than the 50% stenosis, illustrated by the much larger reduction in CVR required to restore the efferent CBF to their normal levels. This is a finding that occurs in a number of simulations, indicating that quite a large stenosis is required (even when in combination with an occlusion), in order to affect cerebral blood flow appreciably.

3.2. RICA Occlusion

The results for the autoregulatory response to the RICA occlusion in combination with a unilateral stenosis are presented in Figure 7. It can be observed that there is a similar pattern to the LICA occlusion where the CBF is not completely restored in the ipsilateral RACA and RMCA, but in this case the reduction in efferent CBF is so great that CVR for these two arteries reaches its lower limit of autoregulation (Figure 7b). As a consequence of this the C_tCO₂ in these arteries remains elevated at the end of the simulation, but by far the more significant result is that with a 70% LICA stenosis, the OEF for the RMCA reaches its upper limit (and very nearly the RACA too) (Figure 6c) meaning that O₂ delivery cannot be maintained to the cerebral territory perfused by the RMCA (Figure 7d).

4. DISCUSSION AND CONCLUSION

The results presented here illustrate only a sample model to which clinical scenarios have been simulated. Since partially or totally occluding an individual's afferent cerebral arteries (or even altering their MABP) while at the same time measuring their efferent CBF presents great practical and ethical problems, validation of the cerebral autoregulation model *in vivo* presents the major limitation of the research at present. Future work will however seek to instead alter arterial blood levels of CO₂ while an individual is in the MRI scanner and hence cause autoregulation to respond in much the same way as if an artery had been occluded. It is an interesting result that an occlusion of the LICA could be tolerated, while an

occlusion of the RICA could not and is a result of the slight asymmetry of the communicating artery diameters and of efferent cerebral blood flow under normal conditions. Other CoW configurations (not presented here) illustrate that the response to a stenosis and/or occlusion also strongly depends upon the configuration (i.e. which if any communicating arteries are absent or hypoplastic) and the normal levels of efferent cerebral blood flow, emphasizing the need for a modelling technique which can take these patient specific variables into account in order to make realistic predictions.

The major difficulty in modelling the vasculature from the carotid bifurcation to the distal CoW is in the computational time required and the scanning time required to include this region with adequate spatial resolution. Future work may involve testing this assumption. In situations where a severe carotid stenosis is already present, the effects of possible turbulence and reduced blood flow can degrade the MR TOF signal, although contrast enhanced MR angiography may still be used in order to generate the 3D model. The focus of the present research however, is more closely aimed at predicting the effects of future stenosis, rather than waiting till they are present before creating the patient specific model, since by this time, the adequacy of the individuals' CoW in providing collateral flow, will already be apparent.

5. REFERENCES

- Alpers, B.J., Berry, R.G., Paddison, R.M. (1959), Anatomical studies of the CoW in normal brain, *Arch Neurol. Psychiatry*, 81, 409-418.
- Banaji, M., A. Tachtsidis, D. Delpy, and S. Baigent (2005), A physiological model of cerebral blood flow control, *Mathematical Biosciences*, 194(2), 125-173.
- Cebral, J. R., M. A. Castro, O. Soto, R. Lohner, and N. Alperin (2003), Blood flow models of the circle of Willis from magnetic resonance data, *Journal of Engineering Mathematics*, 47, 369-386.
- Charbel, F. T., M. D. Zhao, S. Amin-Hanjani, W. Hoffman, X. J. Du, and M. E. Clark (2004), A patient-specific computer model to predict outcomes of the balloon occlusion test, *Journal of Neurosurgery*, 101(6), 977-988.
- David, T., M. Brown, and A. Ferrandez (2003), Auto-regulation and blood flow in the cerebral circulation, *International Journal for Numerical Methods in Fluids*, 43, 701-713.
- Hartkamp, M. J., J. van der Grond, F. E. de Leeuw, J. C. de Groot, A. Algra, B. Hillen, M. M. B. Breteler, and W. P. T. M. Mali (1998), Circle of Willis: Morphologic variation on three-dimensional time-of-flight MR angiograms, *Radiology*, 207(1), 103-111.
- Hillen, B., H. W. Hoogstraten, and L. Post (1986), A mathematical-model of the flow in the circle of Willis, *Journal of Biomechanics*, 19(3), 187-194.
- Kim, C. S. S., C. Kiris, D. Kwak, and T. David (2006), Numerical simulation of local blood flow in the carotid and cerebral arteries under altered gravity, *Journal of Biomechanical Engineering-Transactions of the Asme*, 128(2), 194-202.
- Lorensen, W. E. and C. H. E. (1987), Marching cubes: A high resolution 3d surface construction algorithm, *Computer Graphics*, 21(4), 163-169.
- Newell, D.W., Aaslid, A.A., Lam, A., Mayberg, T.S., Winn, H.R. (1994), Comparison of Flow and Velocity During Dynamic Autoregulation Testing in Humans, *Stroke*, 25, 793-797.
- Strandgaard, S., (1976), Autoregulation of Cerebral Blood Flow in Hypertensive Patients, *Circulation*, 53(4), 720-727.
- Thoman, W. J., S. Lampotang, D. Gravenstein, and J. van der Aa (1998), A computer model of intracranial dynamics integrated to a full-scale patient simulator, *Computers and Biomedical Research*, 31(1), 32-46.
- Ursino, M. (1991), A mathematical-model of overall cerebral blood-flow regulation in the ra, *Ieee Transactions on Biomedical Engineering*, 38(8), 795-807.